PROBING MASSIVE STAR FORMATION WITH THE ATACAMA LARGE MILLIMETER/SUBMILLIMETER ARRAY (ALMA)

Zoie Telkamp[1]

Adele Plunkett[2,3] (Advisor), Jonathan Tan[1,4]

[1]Dept. of Astronomy, University of Virginia [2]National Radio Astronomy Observatory; [3]North American ALMA Science Center; [4]Dept. of Space, Earth & Environment, Chalmers University of Technology

Abstract

Despite the huge impact that high-mass stars have on galaxy environments and the stars and planets that form within them, there is still no consensus on how they form. Some theories pose that their formation is driven by accretion from gravitationally bound disks of gas and dust. While studying the properties of these disks is key to understanding their role in massive star formation, few instruments are powerful enough to probe the scales at which these disks form around massive stars. We performed a systematic search of the Atacama Large Millimeter/submillimeter Array (ALMA) Science Archive to find the highest resolution data available for high-mass protostars (stars still in the formation stage). Using these data, we measured and analyzed 1.3 mm continuum fluxes and morphological features to test predictions of some of the leading models of massive star formation.

Introduction

Massive stars (which have a mass greater than 8 times that of the sun) are critical to the regulation and evolution of galaxy environments. The high energy output of their winds, radiation, and eventual collapse into supernovae impacts a large range of processes, from the reionization of the universe to the formation of other stars and their planets. Yet, in spite of their importance, the mechanisms behind their formation are still disputed. The leading theories of massive star formation include Core Accretion (e.g., Mclaughlin et al. 1997; Mckee et al. 2003; Krumholz et al. 2009) and Competitive Accretion (e.g., Bonnell et al. 2001; Wang et al 2010; Grudic et al. 2022). Core Accretion is basically a scaled-up version of the formation of low-mass stars and theorizes that they form when self-gravitating cores (supported by turbulence and magnetic fields) collapse via a central disk. This is predicted to result in a primary bipolar outflow, as often observed with low mass protostars. Competitive Accretion assumes that massive protostars form towards the centers of globally collapsing protoclusters and compete for material as they accrete gas. Due to close protostellar interactions, protostars under Competitive Accretion will accrete from smaller, truncated disks, and the outflows will be more disordered.

While many disks around low mass protostars have been observed, limited information exists on the properties of their high mass counterparts. This is largely due to the fact that massive protostars are typically located at large distances from us, which means that very high resolutions are required to probe the scale at which their disks would form. The Atacama Large Millimeter/submillimeter Array (ALMA) is powerful enough to make these high-resolution observations. For example, Zhang et al. 2019 resolved a binary system of massive protostars, with evidence of an individual disk around each one. Furthermore, Maud et al. 2019 observed a massive O-type star still undergoing formation and hosting a Keplerian disk.

Given these developments, we have sys-

tematically searched the National Radio Astronomy Observatory's (NRAO) ALMA Science Archive to find the highest resolution ALMA data available for massive protostars. Using such high-resolution data allows us to probe smaller scales (around a few hundred au), where we typically find the disks of massive protostars. With these data, we identified over 100 sources, measured their 1.3 mm continuum fluxes, and estimated properties of their potential disks to test predictions of massive star formation theories.

Methods

Data Selection

Located on the Chajnantor plateau in Chile, ALMA is a radio telescope used to observe light at millimeter and submillimeter wavelengths. ALMA consists of 66 antennas, with its main array possessing 50 dishes that are each 12 meters in diameter and act together as a single telescope. These antennas can be arranged in different configurations to probe different scales of astronomical objects. To investigate the scales at which the disks of massive protostars are potentially present, we needed to use high-resolution "long baseline" data gathered using configurations where the arrays are spaced farther apart.

To obtain these data, we utilized the NRAO ALMA Science Archive, which hosts >70,000 observations of objects spanning planets and stars, to distant galaxies. Since massive protostars are often located several kiloparsecs away and their disks are typically expected to be seen at scales of a few hundred au, we restricted our search to data with an angular resolution under 0.05". A search for Band 6 continuum data with this resolution and under the "High-mass star formation" keyword yielded 42 publicly available observations at the time of our search. Next, we visually inspected these images and selected those with a primary source that appeared relatively compact and isolated, resulting in 18 final images, some of which contained multiple sources. The names, coordinates, and distances of the regions covered by these images are shown in Table 1.

Source Identification

Next, we used the Astrodendro Python package (Robitaille et al. 2019) to identify sources in the images without primary beam correction. This package identifies hierarchical structures in the input data and returns their locations and estimated sizes. We considered the highest level structures, or "leaves" within the 30% primary beam response as our source candidates. We set the minimum flux density of a source to be 5 times the noise level of the corresponding image and the minimum size as the synthesized beam area. To filter out non-compact sources or close multiples, we removed any sources connected to another source through a lower-level structure. In order to obtain sufficiently isolated sources for our analysis, we also removed any sources with a neighbor closer than 2 beam radii. The resulting sample contained 130 sources.

2-Dimensional Gaussian Fitting

The images in our dataset span physical resolutions of $\sim$20-300 au. Since we expect to find the disks of massive protostars at these scales, we attribute the observed emission in each image to a potential disk (called "disk candidates" in the rest of this paper) with possible envelope contributions. To characterize these disk candidates, we search for the elongation of compact continuum structures in the data by fitting a 2-dimensional elliptical Gaussian to each source in the primary beam corrected images. We used the imfit task of the Common Astronomy Software Applications for Radio Astronomy (CASA) (CASA Team et al. 2022) (version 6.4.1) to perform the fitting on a window centered on each source. The outputs included the estimated position and integrated flux of each source, as well as the position angle and full width at half maximum (FWHM) of the major

Name	R.A.(J2000)	Decl.(J2000)	d (kpc)	Angular Res. (")
G032.03+00.05	$18^h49^m37^s.05$	$-00°46'50".22$	5.5[1]	0.03
G11.92-0.61	$18^h13^m58^s.11$	$-18°54'20".14$	3.4[2]	0.03
G14.22-0.50	$18^h18^m12^s.99$	$-16°57'21".82$	3.7[3]	0.05
G24.60+0.08	$18^h35^m40^s.50$	$-07°18'34".02$	3.5[4]	0.05
G339.88-1.26	$16^h52^m04^s.65$	$-46°08'34".00$	2.1[5]	0.05
G35.2N	$18^h58^m13^s.03$	$+01°40'36".14$	2.2[6,7]	0.03
G351.77-0.54	$17^h26^m42^s.57$	$-36°09'17".60$	1.0[8]	0.02
G353.273+0.641	$17^h26^m01^s.59$	$-34°15'14".94$	1.7[9]	0.02
G45.47+0.05	$19^h14^m25^s.74$	$-11°09'25".90$	8.4[10]	0.03
IRAS 07299-1651	$07^h32^m09^s.67$	$-16°58'14".00$	1.7[11]	0.03
IRAS 18337-0743	$18^h36^m40^s.82$	$-07°39'17".74$	3.8[12]	0.05
NGC 6334 I N	$17^h20^m54^s.90$	$-35°35'10".02$	1.3[13,14]	0.04
R Mon	$06^h39^m09^s.95$	$+08°44'09".55$	0.8[15]	0.03
S255 IR	$06^h12^m54^s.02$	$+17°59'23".10$	1.6[16]	0.03
c20kms^{-1} c1	$17^h45^m37^s.55$	$-29°05'44".23$	8.1[17]	0.02
c20kms^{-1} c4	$17^h45^m37^s.57$	$-29°05'44".23$	8.1[17]	0.02
Sgr C	$17^h44^m40^s.37$	$-29°28'14".79$	8.1[17]	0.02

Table 1 : ALMA source name, RA and DEC of the central coordinates, distance, and angular resolution of each observation in the sample. Distance references: (1) Battersby et al. 2014; (2) Sato et al. 2014; (3) Rathborne et al. 2006; (4) Moscadelli et al. 2021; (5) Krishnan et al. 2015; (6) Zhang et al. 2022; (7) Wu et al. 2014; (8) Leurini et al. 2011; (9) Neckel et al. 1978; (10) Wu et al. 2019; (11) Reid et al. 2009; (12) Lu et al. 2014; (13) Reid et al. 2014; (14) Chibueze et al. 2014; (15) Jones & Herbig 1982; (16) Burns et al. 2016; (17) Gravity Collaboration et al. 2019.

and minor axes of the 2D Gaussian fit before and after the image is deconvolved from the synthesized beam. We defined "poor" fits as those with a residual image standard deviation greater than 2 times the standard deviation of the input image. This resulted in a final sample of 102 sources.

Estimating Disk Properties

We used the 2D Gaussian fits to estimate the orientation, radius, inclination, and mass of each disk candidate. First, we defined the expected disk axis as the axis of elongation of a source in the corresponding continuum image. As such, we took the position angle of each 2D Gaussian fit as the projected disk major axis direction. Next, we used the 2D Gaussian fits to estimate the radius of each disk candidate. Following Ansdell et al. 2016, we defined the radius of a disk as the radial point that encompasses 90% of the total flux density, approximately corresponding to the 2σ point of a Gaussian (see Tobin et al. 2020 for discussion of the assumptions made in, and limitations of, this method.). We used the FWHM values outputted by CASA to obtain the σ of the major axis of each fit in arcseconds and multiplied by the distance to the source (obtained through a literature search) to calculate a radius in au. To estimate the inclination of each system, we assumed a circularly symmetric disk and used the following equation:

$$i = \cos^{-1}(b/a), \quad (1)$$

where i is the inclination and a and b are the lengths of the major and minor axes of the 2D Gaussian fit.

Next, we used the CASA-outputted flux density of each source and some simplifying assumptions to help constrain the masses of the identified structures. Disks around massive protostars are sometimes marginally optically thick, and their temperature is not necessarily constant throughout. However, assuming optically thin emission and constant temperature yields a lower bound estimate for the mass of each disk candidate. Under these assumptions, the dust mass can be calculated with the following equation:

$$M_{dust} = \frac{S_\nu d^2}{\kappa_\nu B_\nu(T)}, \quad (2)$$

where d is the distance to the source, κ_ν is the opacity, S_ν is the flux density measurement, and B_ν is the blackbody distribution flux at 1.3 mm for a dust temperature T. We performed these calculations at 70K, which is the average envelope temperature within $\sim$10,000 au around a $12-16$ solar mass protostar derived from radiative transfer simulations (Zhang & Tan 2018). We used an opacity of $\kappa_{1.3mm} = 0.89$ cm$^2 g^{-1}$, which Ossenkopf & Henning 1994 estimated at 1.3 mm for ice-covered dust grains with an ice-to-silicate ratio of 1.2. To calculate the total lower bound mass of the gas and dust for each disk candidate (with some potential envelope contributions), we used a gas-to-dust mass ratio of 100, which is typically assumed for the interstellar medium.

Results and Future Work

Three of the regions in our sample (c20 kms^{-1} c1, c20 kms^{-1} c4, and Sgr C) are located in the Central Molecular Zone (CMZ), a region spanning the center of the Milky Way galaxy. The CMZ is known to exhibit extreme conditions including higher temperatures, densities, and stronger magnetic fields (e.g., Henshaw et al. 2023). In addition, the CMZ is located at a farther distance than the rest of the regions in our sample, so we are potentially probing larger-scale physical structures or facing greater envelope contributions in these observations. Because of these discrepancies, we present the CMZ results separate from, and in comparison to, the rest of our sample. Figure 1 shows the distributions of the radii of the disk candidates calculated from the images convolved with the synthesized beam (left) and deconvolved from the beam (right). From these plots, we can see that the radii span a few hundred au to almost 2000 au. All of the disk candidates in the non-CMZ regions have a calculated radius of <500 au, whereas the CMZ radii tend to be larger and host the largest values in the sample. It is possible that the chaotic nature of the CMZ results in these larger radii. However, these radii are just lower limits, and since the CMZ is farther away than most of the other regions, the CMZ observations probe larger spatial scales ($\sim$300 au), while many of the other observations probe sub-100 au spatial scales. Figure 2 shows these radii divided by the corresponding synthesized beam radii. From these plots, we can see that the difference between the beam-normalized radii distributions for the CMZ and non-CMZ sources is much less drastic. This indicates that caution must be employed when comparing the disk properties between these populations.

Figure 3 shows the inclination estimates for these systems. The CMZ and non-CMZ sources distributions appear comparable upon visual inspection, and we see that neither distribution follows a random uniform distribution in cosine. However, it is important to note that these inclinations are calculated assuming vertically thin disks, and modeling is needed in order to assess the impact of their actual thickness on the computed inclinations. This distribution can also reflect the systematic biases in the ALMA archive. For example, brighter sources are more likely to be observed, and fewer observations exist for edge-on disks.

Figure 4 shows the fluxes measured for the sources and the resulting lower bound disk

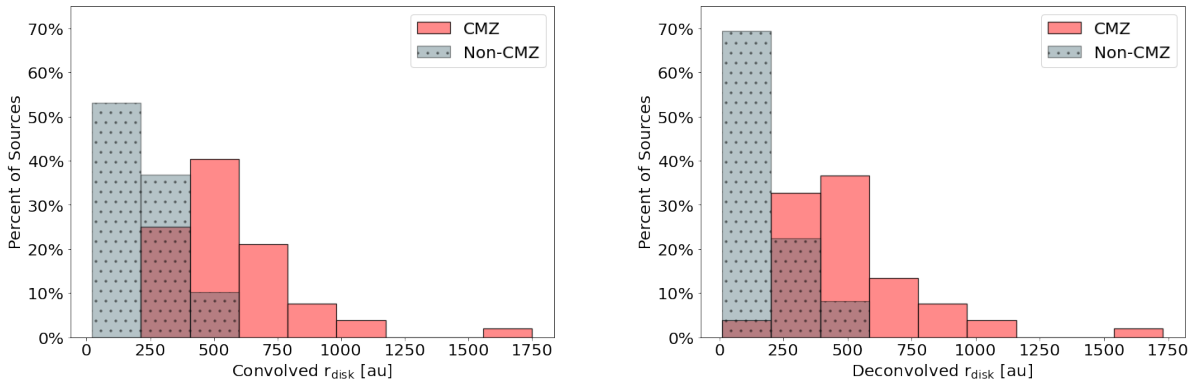

Figure 1 : Distributions of the calculated disk radii of the sources in the sample, separated into sources located within within the CMZ (solid pink histogram) and sources not in the CMZ (dotted blue histogram). The left plot shows the radii calculated from the 2D Gaussian fits before each image was deconvolved from its synthesized beam, and the right plot shows the radii calculated from the fits after beam deconvolution.

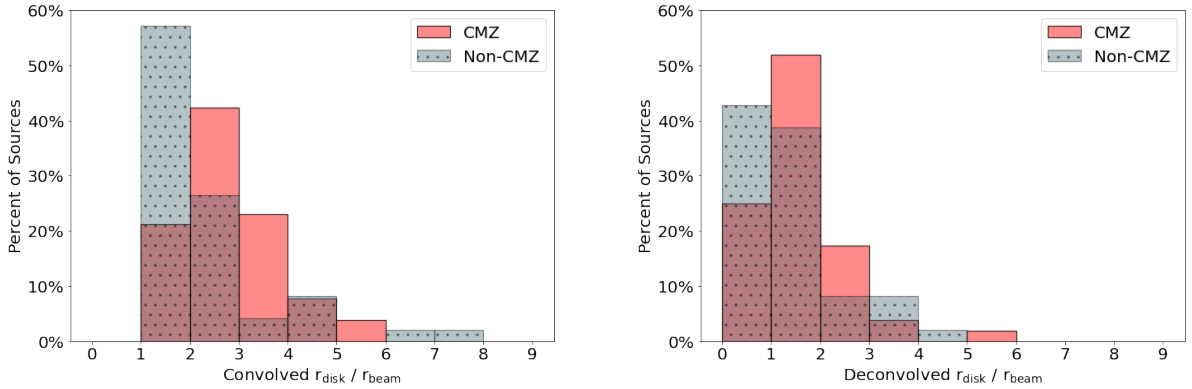

Figure 2 : Distributions of the calculated synthesized beam-normalized radii of the sources in the sample before (left) and after (right) beam deconvolution.

mass estimates. Here, we see that the CMZ distribution is shifted to slightly lower fluxes, which could be due to the fact that it is farther away than the rest of the sample. We also see that the CMZ mass distribution is shifted towards higher values, again noting that these observations probe larger spatial scales and could be subject to greater envelope contributions. The next step will be to compare these distributions to distributions of protostellar disk sizes and masses observed in lower mass surveys such as in Tobin et al. 2020.

Another goal of this project is to compare disk and outflow axes of massive protostars to assess trends in their relative orientations. Multiple studies have shown that bipolar outflows are observed in 50-80% of their samples of high mass protostars (e.g., Henning et al. 2000; Zhang et al. 2001; Ridge et al. 2001). However, different models of massive star formation make contrasting predictions of the morphology and abundance of these outflows. For

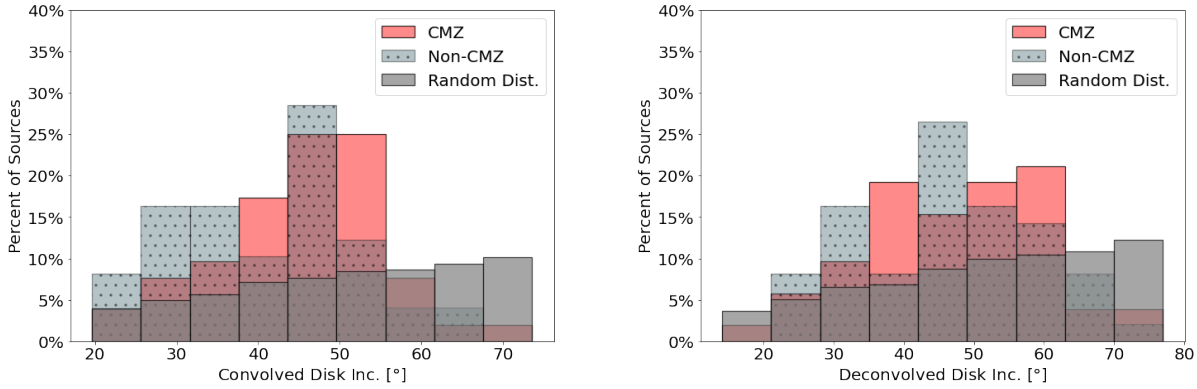

Figure 3 : Distributions of the disk inclinations of the sources in the sample before (left) and after (right) beam deconvolution. A random distribution in cosine is overplotted for comparison

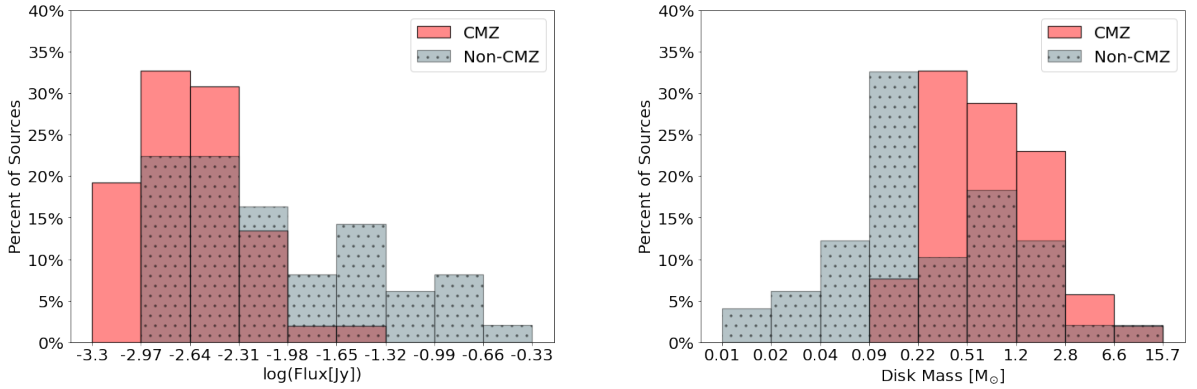

Figure 4 : Distributions of the log of the fluxes (in Janskys) outputted for each source by CASA and the lower bound disk candidate masses (in solar masses) calculated from these.

example, if stars form via Core Accretion, disk winds are assumed to result in the presence of a "primary" bipolar outflow. If stars form via Competitive Accretion, the processes involved are more chaotic, and the high density of low-mass protostars will produce strong dynamical interactions that result in more disordered outflows.

As previously described, we estimated the orientation of each disk candidate in our sample using the elongation of the corresponding 2D Gaussian fit. To obtain outflow axis estimates, we are performing a literature search to obtain information on CO outflows associated with our sample and their reported directions. An example comparison is shown in Figure 5. With this information, we will perform a statistical analysis to assess the significance of any preferential relative orientation from a total random distribution using tests such as a projected Rayleigh statistic and Kolmogorov–Smirnov test. We can then compare any observed trends to the predictions made by the leading massive star formation theories.

Summary and Conclusions

Massive stars have a large influence on galactic environments, impacting the formation

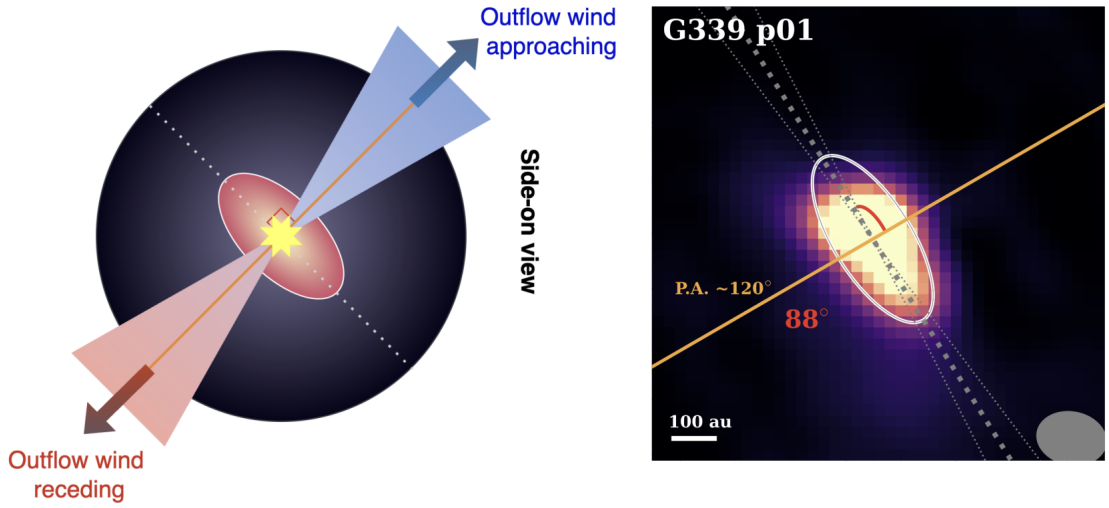

Figure 5 : Example comparison between the estimated disk axis and outflow axes. The left image shows the orthogonal alignment predicted by the Core Accretion theory, where the yellow star represents the protostar, the pink ellipse represents the disk, the dotted white line shows the disk axis, and the orange line shows the outflow axis. The right image follows these same conventions and shows a real image of source G339 with an angle of 88° between the disk and outflow axes. The narrow grey lines on either side of the predicted disk axis represent the uncertainty. A 100 au scale bar is shown in the lower left, and the synthesized beam is represented by the grey ellipse in the lower right.

and evolution of other stars and planets. In spite of their importance, the mechanisms through which they form—whether it occurs through a scaled-up version of low-mass star formation, or a competitive accretion process within globally collapsing clusters of protostars—is still uncertain. Testing predictions of protostellar properties and environment can provide insight into these formation mechanisms. Taking advantage of the high-resolution observations enabled by ALMA, we can zoom into scales at which we expect to find the disks of these massive protostars. Here, we have presented some preliminary results of a uniform analysis of some of the highest resolution ALMA data of massive protostars to date and discussed some potential trends among the radii, masses, and inclinations of their potential disks. Through continued statistical analysis of these results and comparison with existing protostellar surveys, we aim to provide further constraints on the massive star formation process.

Acknowledgements

This work is supported by the Virginia Space Grant Consortium Graduate Research STEM Fellowship Program, the National Radio Astronomy Observatory (NRAO) Summer Student Research Assistantship Program, the NRAO Graduate Student Researcher Program, and the North American ALMA Science Center.

REFERENCES

Ansdell, M., Williams, J. P., van der Marel, N., et al. 2016, The Astrophysical Journal, 828, 46, doi: 10.3847/0004-637X/828/1/46

Battersby, C., Ginsburg, A., Bally, J., et al. 2014, ApJ, 787, 113, doi: 10.1088/0004-637X/787/2/113

Beuther, H., Schilke, P., Sridharan, T. K., et al. 2002, A&A, 383, 892, doi: 10.1051/0004-6361:20011808

Bonnell, I. A., Bate, M. R., Clarke, C. J., & Pringle, J. E. 2001, MNRAS, 323, 785, doi: 10.1046/j.1365-8711.2001.04270.x

Burns, R. A., Handa, T., Nagayama, T., Sunada, K., & Omodaka, T. 2016, MNRAS, 460, 283, doi: 10.1093/mnras/stw958

CASA Team, Bean, B., Bhatnagar, S., et al. 2022, PASP, 134, 114501, doi: 10.1088/1538-3873/ac9642

Chibueze, J. O., Omodaka, T., Handa, T., et al. 2014, ApJ, 784, 114, doi: 10.1088/0004-637X/784/2/114

GRAVITY Collaboration, Abuter, R., Amorim, A., et al. 2019, A&A, 625, L10, doi: 10.1051/0004-6361/201935656

Grudić, M. Y., Guszejnov, D., Offner, S. S. R., et al. 2022, MNRAS, 512, 216, doi: 10.1093/mnras/stac526

Henning, T., Schreyer, K., Launhardt, R., & Burkert, A. 2000, A&A, 353, 211

Henshaw, J. D., Barnes, A. T., Battersby, C., et al. 2023, in Astronomical Society of the Pacific Conference Series, Vol. 534, Protostars and Planets VII, ed. S. Inutsuka, Y. Aikawa, T. Muto, K. Tomida, & M. Tamura, 83, doi: 10.48550/arXiv.2203.11223

Jones, B. F., & Herbig, G. H. 1982, AJ, 87, 1223, doi: 10.1086/113205

Krishnan, V., Ellingsen, S. P., Reid, M. J., et al. 2015, The Astrophysical Journal, 805, 129, doi: 10.1088/0004-637X/805/2/129

Krumholz, M. R., Klein, R. I., McKee, C. F., Offner, S. S. R., & Cunningham, A. J. 2009, Science, 323, 754, doi: 10.1126/science.1165857

Leurini, S., Codella, C., Zapata, L., et al. 2011, A&A, 530, A12, doi: 10.1051/0004-6361/201016190

Lu, X., Zhang, Q., Liu, H. B., Wang, J., & Gu, Q. 2014, ApJ, 790, 84, doi: 10.1088/0004-637X/790/2/84

Maud, L. T., Cesaroni, R., Kumar, M. S. N., et al. 2019, A&A, 627, L6, doi: 10.1051/0004-6361/201935633

McKee, C. F., & Tan, J. C. 2003, ApJ, 585, 850, doi: 10.1086/346149

McLaughlin, D. E., & Pudritz, R. E. 1996, JRASC, 90, 326

Moscadelli, L., Cesaroni, R., Rioja, M. J., Dodson, R., & Reid, M. J. 2011, A&A, 526, A66, doi: 10.1051/0004-6361/201015641

Neckel, T. 1978, A&A, 69, 51

Ossenkopf, V., & Henning, T. 1994, A&A, 291, 943

Rathborne, J. M., Jackson, J. M., & Simon, R. 2006, The Astrophysical Journal, 641, 389, doi: 10.1086/500423

Reid, M. J., Menten, K. M., Brunthaler, A., et al. 2009, ApJ, 693, 397, doi: 10.1088/0004-637X/693/1/397

—. 2014, ApJ, 783, 130, doi: 10.1088/0004-637X/783/2/130

Ridge, N. A., & Moore, T. J. T. 2001, AA, 378, 495, doi: 10.1051/0004-6361:20011180

Robitaille, T., Rice, T., Beaumont, C., et al. 2019, astrodendro: Astronomical data dendrogram creator, Astrophysics Source Code Library, record ascl:1907.016. http://ascl.net/1907.016

Sato, M., Wu, Y. W., Immer, K., et al. 2014, The Astrophysical Journal, 793, 72, doi: 10.1088/0004-637X/793/2/72

Tobin, J. J., Sheehan, P. D., Megeath, S. T., et al. 2020, The Astrophysical Journal, 890, 130, doi: 10.3847/1538-4357/ab6f64

Wang, P., Li, Z.-Y., Abel, T., & Nakamura, F. 2010, ApJ, 709, 27, doi: 10.1088/0004-637X/709/1/27

Wu, Y. W., Reid, M. J., Sakai, N., et al. 2019, The Astrophysical Journal, 874, 94, doi: 10.3847/1538-4357/ab001a

Wu, Y. W., Sato, M., Reid, M. J., et al. 2014, A&A, 566, A17, doi: 10.1051/0004-6361/201322765

Zhang, Q., Hunter, T. R., Brand, J., et al. 2001, ApJL, 552, L167, doi: 10.1086/320345

Zhang, Y., & Tan, J. C. 2018, ApJ, 853, 18, doi: 10.3847/1538-4357/aaa24a

Zhang, Y., Tan, J. C., Tanaka, K. E. I., et al. 2019, Nature Astronomy, 3, 517, doi: 10.1038/s41550-019-0718-y

Zhang, Y., Tanaka, K. E. I., Tan, J. C., et al. 2022, ApJ, 936, 68, doi: 10.3847/1538-4357/ac847f